Mesoporous Poly(benzimidazole) Networks *via* Solvent Mediated Templating of Hard Spheres

Jens Weber, Markus Antonietti, and Arne Thomas*

Department of Colloid Chemistry, MPI of Colloids and Interfaces, Research Campus Golm, D-14424 Potsdam, Germany

Received November 10, 2006; Revised Manuscript Received November 21, 2006

ABSTRACT: Mesoporous Poly(benzimidazole) with well-defined porosity and pore diameter of 11 nm was synthesized via a hard templating approach using silica nanoparticles as template. The effect of the template concentration as well as the influence of the cross-linking density on the resulting pore structure was investigated. The samples were characterized by small-angle X-ray scattering and nitrogen sorption, revealing a linear increase of the porosity and surface area with increasing content of the template up to a critical concentration. Exceeding this concentration leads to a breakdown of some pores due to the emerging high interfacial energy. The effect of the cross-linking density was shown to be nonlinear. Samples with more than 20 mol % cross-linker revealed perfect replication of the template, while a lower cross-linking density leads to a breakdown of some pores.

Introduction

Porous polymers have found widespread applications in membrane technologies, as insulators, ion exchange resins, and separation media and their application as high tech materials for sensors, artificial antibodies and opto-electronic devices is currently being explored.[1] Porosity in polymers means mostly micro- or macroporosity and often describes polydisperse pore sizes with average diameters in the nanometer regime, rather then a distinct porosity with defined pore sizes. In general, porosity in polymers is achieved due to inert porogens or templates present during synthesis and cross-linking of the polymer framework around them.[1] These templates can be not only solvent molecules ("solvent pores"), surfactants or polymers and their micelles and lyotropic phases ("soft templates") but also hard inorganic nanoparticles ("hard templates"). For soft templates the control of the resulting pore size is rather difficult, since thermodynamic incompatibility of the low molecular weight templates with the forming polymer phase results often in demixing.[2,3] Consequently, the diameter of these pores range from a few hundred nanometers to the micrometer range and result in surface areas of around 10 m^2/g—orders of magnitude less than inorganic porous materials exhibiting micro- or mesoporosity (>1000 m^2/g). Solvent pores, on the other hand, are extremely small, improve only gas transport, but trap solvents.[4] Different other synthetic strategies were also used to realize porous polymer networks. Gases, liquids and supercritical CO_2 were employed for pore generation,[5−7] furthermore thermally and chemical induced phase separation.[8−11]

In comparison far less regular mesoporous polymers have been synthesized. Recently, lyotropic phases have been used for the synthesis of ordered mesoporous phenolic resins by two research groups.[12,13] However, soft templates are not applicable in the synthesis of polymers, which require harsh polymerization conditions.

"Hard templates" such as colloidal silica particles proved to be beneficial for the synthesis of nanostructured polymer resins, because of a number of reasons. First, their chemical and thermal inertness allows polymer synthesis under the mentioned conditions. Second, as hard templates they cannot change their shape under altered thermodynamic conditions. Third, they are easy to remove from the final polymer phase. Johnson et al. synthesized ordered mesoporous polymer resins based on divinylbenzene and ethylene glycol dimethyl acrylate, respectively, using assembled silica spheres as template.[14] Also the replication of mesoporous silicas into polymers and into carbon was exploited.[15−18] However, the expansion of this approach has scarcely been exploited for high-performance polymers,[19] even though a distinct mesoporosity might enhance the already broad applicability of these polymers. One of this polymers is poly(benzimidazole) (PBI), which possesses a high thermal and chemical stability interesting for a large variety of applications including electronic and automotive components, structural resins, and fire resistant materials.[20] In addition, through the imidazole rings, PBI supports extended H-bridge system, which makes membranes of PBI, especially when doped with acids, to good proton conductors. PBI has therefore high potential for applications in proton exchange membrane fuel cells (PEMFCs).[21−23] Especially in direct methanol fuel cells, which are recognized as one of the most promising alternative power sources for the transportation sector, they have several advantages compared to the commonly used perfluorosulfonic acid membranes, due to their high cost and low performance at temperatures higher than 100 °C. Recently, Mecerreyes et al. reported on the introduction of porosity into PBI.[24] By leaching out a low molecular weight compound (the porogen), PBI membranes with up to 75% porosity were generated. This approach yielded in a macroporous PBI and the observed pore sizes exhibit rather high dispersity. After doping with phosphoric acid, a linear increase of the ionic conductivity with the initial porosity was observed, most probably due to the remarkable increase of the acid uptake.

Herein, we introduce a general method that allows the synthesis of mesoporous PBI with defined pore size and controlled porosity. PBI is typically synthesized either in melt polycondensation procedures[25,26] or in polyphosphoric acid at 200 °C.[27] These rather harsh conditions make the introduction of a defined porosity into the PBI a difficult task and hardly possible by the commonly used approaches. To overcome these obstacles a solvent mediated hard-templating approach was developed leading to a general pathway for the nanostructuring of poly(benzimidazole). A well-defined 13 nm silica nanosol

* Corresponding author. E-mail: Arne.Thomas@mpikg.mpg.de.

10.1021/ma062598m CCC: $37.00
Published on Web 01/24/2007

Scheme 1. General Principle of the Hard-Templating Approach for the Generation of Mesoporous Polymers

was used as a template to generate a continuous porosity within PBI. As PBI is a glassy, noncrystalline polymer, it is to be expected that small pores simply heal out or are getting closed because of capillarity, especially at high temperatures, when contacted with solvents or plasticizing gases. Therefore, a new, highly cross-linked PBI resin was synthesized, essentially by incorporating a trifunctional carboxylic acid monomer into the network. The porosity of this resin was compared with linear PBI and various copolymers of the two.

The resulting nanostructured PBI networks with controlled porosity, high surface area, functionality, and high-temperature resistance were characterized by TEM, porosimetry, and quantitative SAXS measurements, thus setting up a model system to analyze mesoporosity in polymer system, which up to now still depends on assumptions.

Results and Discussion

Synthesis of Mesoporous Poly(benzimidazole) Networks via Silica Hard Templating. Mesoporous PBI's were synthesized combining the hard templating approach and the classical melt polycondensation of PBI.[25] The general concept of this approach is depicted in Scheme 1.

The standard way of preparing mesoporous polymers by hard templating is to mix the liquid monomers with solid nanoparticles.[14] However, the monomers used in the synthesis of PBI are solid up to 170 °C. At this temperature the diverse phenyl ester compounds are melting, and the 3,3′-diaminobenzidine is dissolved in the melt.

Silica nanoparticles with a diameter of about 13 nm are commercially available as a 40 wt % dispersion in water under the trademark LUDOX HS-40 and have been used recently for the synthesis of a mesoporous carbon nitride.[28] Silica was chosen as we learned in this previous work that it disperses nicely in aminic solvents, i.e., clear, non-opaque "solutions" are formed, indicating the absence of both particle aggregation and demixing.

In a first experiment the LUDOX dispersion was mixed with the monomers, and the mixture was heated up to 180 °C. However, this resulted in an intermediate solid-state due to water evaporation, which yields at least partially in a segregation of the monomers and the silica nanoparticles and subsequently in a low homogeneity and low porosity of the final polymers. To accomplish better mixing under those high template concentrations and to disperse the silica nanoparticles homogeneous within the monomers, DMF was used as a mediator. By heating a mixture of the monomers, LUDOX dispersion, and DMF to 100 °C, we observed the formation of a clear, brown solution, showing complete dissolution of the monomers as well as the homogeneous dispersion of the silica particles in DMF (Figure S1). This solution could be molded and shaped to the desired form, including membrane films.

Further heating to 160 °C under an argon-flow leads to evaporation of the solvent while the polycondensation starts. By application of reduced pressure and heating to 200 °C for 1.5 h, residual DMF is evaporated and the reaction has progressed to larger extents. Finally, the resulting solid has to be heated up to 400 °C under N_2-atmosphere for 0.5 h to achieve complete ring closure. The template was removed by treating the hybrids with 4 M NH_4HF_2 solution for 3 days, followed by exhaustive washing with water and ethanol.

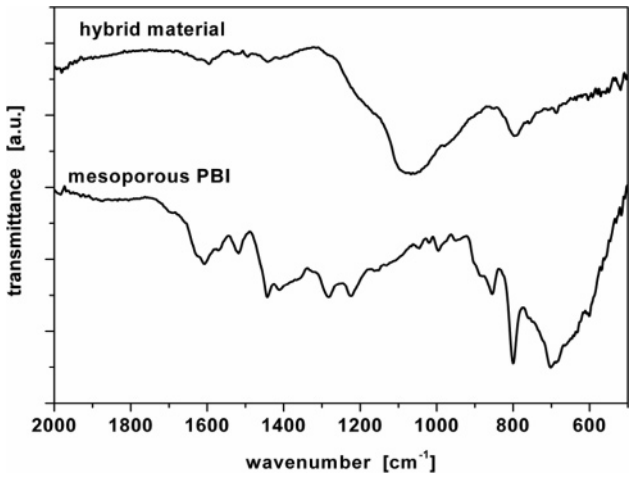

Figure 1. Typical ATR−IR spectra of the hybrid material and the mesoporous PBI after removal of the silica.

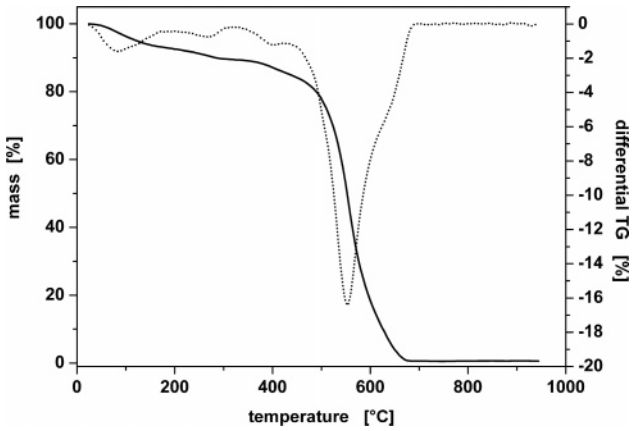

Figure 2. Thermogravimetric analysis of a fully cross-linked porous PBI.

Figure 1 shows typical IR spectra of the silica−PBI composite and the porous PBI. It can be seen that the typical SiO_2 absorption band at 1070 cm^{-1}, observable in the hybrid material, has disappeared in the pure PBI. The absence of a strong carbonyl absorption band shows that the ring closure to the imidazole has been completed. The IR spectra of the porous PBI shows the characteristic features of PBI as reported in the literature.[25,29]

Furthermore, TGA measurements proved that the silica was completely removed from the samples. Figure 2 shows a typical TGA curve. The first weight loss is due to the well-known water uptake of PBI,[30] the main weight loss at a temperature of about 550 °C shows the high-temperature resistance of the cross-linked PBI. The 100% mass loss up to 700 °C underlines clearly that the porous PBI contains no residual silica.

Scheme 2. Synthesis and Chemical Structure of Cross-Linked Poly(benzimidazole)

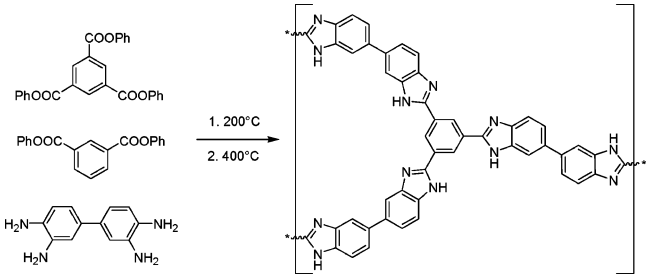

Variation of the Template Content. In order to prevent pore collapsing because of the high interfacial energy and capillarity, mesoporous polymers are usually highly cross-linked. Since the porosity and surface area is controlled by the amount of the silica template, we investigated first the effect of the template content with a fully cross-linked PBI. For this purpose, benzene-1,3,5-tricarboxylic acid triphenyl ester was used as a three-functional monomer in the synthesis of PBI. To the best of our knowledge, this is the first time that this trifunctional cross-linker is introduced for the generation of a PBI resin. The silica/polymer weight ratio was varied from 0.3 to 1.27. The structure of the cross-linker, benzene-1,3,5-tricarboxylic acid triphenyl ester, and of the resulting PBI network are shown in Scheme 2.

The resulting materials were characterized by BET, TEM, and SAXS measurements. Figure 3 shows the nitrogen sorption isotherms of the mesoporous PBIs produced with varying template content.

Nitrogen sorption measurements show type IV isotherms with H1 hysteresis loops indicative for mesoporous materials with a narrow distribution of pore sizes.[31] Furthermore, it can be concluded that the pores are interconnected and freely accessible to nitrogen and that the amount of micropores in PBI networks is very low. The porosity and surface area is increasing linearly with the amount of used template, however the highest porosity is achieved for a silica/polymer ratio of about 1. By exceeding this value, a smaller surface area and less defined pores are observed as indicated by the lowering and broadening of the hysteresis loop. The quantitative results of the nitrogen sorption measurements are summarized in Table 1.

A further insight into the structure of the resulting PBIs was enabled by TEM measurements on microtomed (Figure 4) and bulk samples (Figure S2).

The TEM micrographs reveal the preservation of the pore system in the cross-linked PBI. Spherical mesopores with a diameter slightly smaller than the used silica nanoparticle template are observed, proving the about exact replication of the template. For samples with very low template content (mpPBI-1), we found some agglomeration of the pores, indicating some aggregation of the template particles during the synthesis. For all other samples, the distribution of the pores in the film is disordered, but homogeneous throughout the specimen, as it would be expected from a nonaggregated silica nanosol.

Quantitative small-angle X-ray scattering (SAXS) is presumably the most detailed technique for the characterization of mesoporous materials.[32] Beside determination of the mean pore size and the specific surface area by SAXS, one can also access mutual pore order, average wall thickness and an indirect measure for pore roughness.

It was not possible to fit the scattering curves by applying a model developed for disordered polydisperse spheres,[33] without deviations at low scattering vectors due to the underestimation of the structure factor by the model (see Figure 5). However, the structure factor is too small to allow the fitting of the small angle data with the Percus−Yevick-approach for weakly interacting hard spheres without using physically wrong parameters.[34,35]

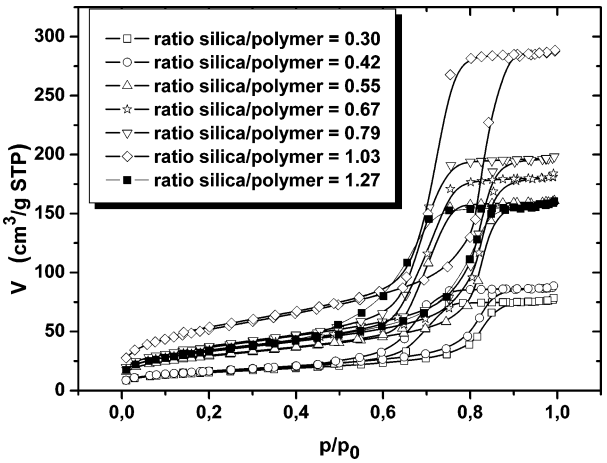

Figure 3. N_2 sorption isotherms for PBI of varying silica/polymer feed ratios.

For a better description of the scattering curve, but also to reveal more information from the SAXS curve than only the size of the domains responsible for the scattering, we essentially followed procedures introduced by Porod.[36] The Porod length l_p is connected to the interface between the two phases and allows the determination of the specific surface area and the average pore size. We used a new method to calculate l_p.[37] Here, the experimental scattering curve $I(s)$ is fitted by a set of basis functions. The parameters of the fit give direct access to the so-called chord-length distribution $g(r)$, which is a quantitative statistical description for the distances connecting phase boundaries in a two-phase system.[37] The advantage of $g(r)$ is that it refers to real space rather than to reciprocal space. However, it is a normalized function, and thus its illustrative power is limited. From the plot of $r \cdot g(r)$, one gets a good visualization of the structures that account to l_p (compare eq 1). Furthermore, the value of the $g(r)$ at $r = 0$, $g(0)$, gives additional information about the roughness of the surface.

The Porod length is the first moment of $g(r)$ and is easily calculated as

$$l_p = \int_0^\infty r \cdot g(r)\, dr \tag{1}$$

The specific surface of a porous system is determined as

$$\frac{S}{V} = \frac{4\phi(1-\phi)}{l_p} \tag{2}$$

Figure 5 shows a typical scattering curve together with the fit obtained by applying the polydisperse spheres model and the fit obtained by the latter approach. It is obvious that the parametrization method, which includes broader physical phenomena gives a more accurate fit. We therefore compared the results obtained by the new technique with the classical method of l_p determination and found at the end rather similar results. All SAXS data were quantified by the more stable and coherent parametrization approach. Table 2 summarizes the obtained numerical results with respect to varying template content.

The calculated surface areas are in good agreement with the results of the N_2 sorption. This proofs that nearly all pores are

Table 1. Results of the Nitrogen Sorption Measurements

sample	ratio silica/polymer	BET surface area [m^2/g]	BJH pore vol [cm^3/g]	micropore vol [cm^3/g]	ϕ_{pore}[a]	BJH av pore diam[b] [nm]
mpPBI-1	0.303	55	0.123	0.0025	0.140	9.23
mpPBI-2	0.424	60	0.139	0.0008	0.154	8.77
mpPBI-3	0.545	105	0.252	0.0032	0.249	9.40
mpPBI-4	0.667	120	0.288	0.0032	0.275	9.23
mpPBI-5	0.788	133	0.311	0.0022	0.289	8.88
mpPBI-6	1.030	188	0.451	0.0029	0.371	9.26
mpPBI-7	1.273	120	0.252	0	0.247	7.68

[a] ϕ is the volume fraction of pores with $\rho_{PBI} = 1.3$ g·cm^{-3}. [b] Using the adsorption branch.

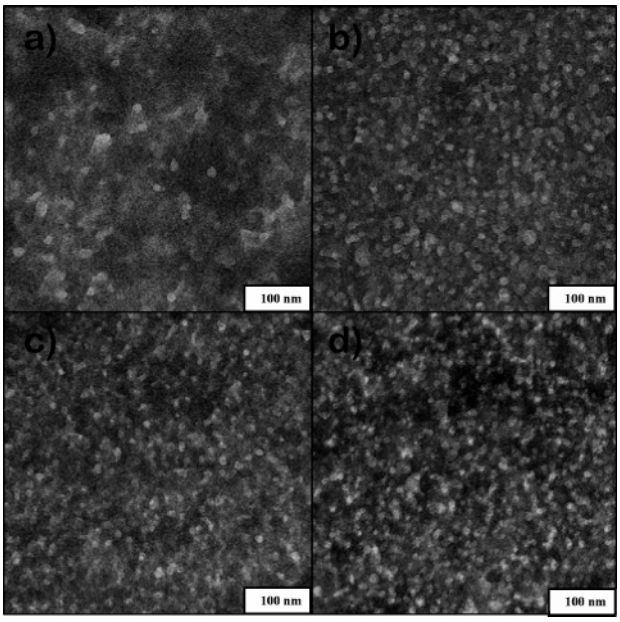

Figure 4. TEM micrographs of ultrathin cuts of mesoporous PBI networks after removal of the template: (a) mpPBI-1: (b) mpPBI-3; (c) mpPBI-6; (d) mpPBI-7.

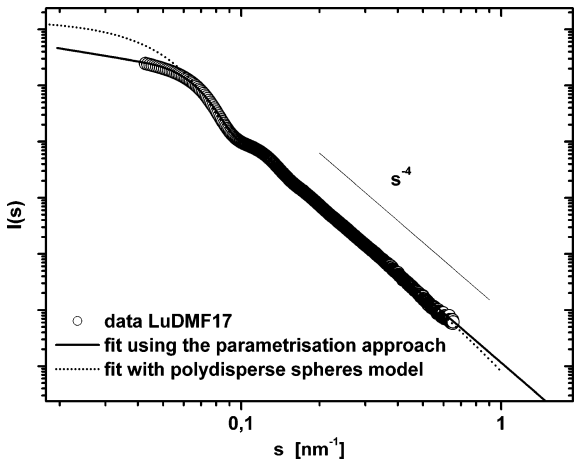

Figure 5. Experimental data and the fit for a system of noninteracting, polydisperse spheres ($R_{sphere} = 6.7$ nm, $\sigma = 1.5$) and the fit obtained by the parametrization method.

accessible. It is known from percolation theory, that there is a threshold value for pore connectivity, if the pore distribution is homogeneous. By TEM, we observed agglomeration of pores for samples with low template content. Pores that are bundled in such agglomerates are connected and thus accessible to N_2, which explains why we do not observe a threshold value for the pore connectivity.

Furthermore, the good agreement of both methods with the theoretical surface area, that is calculated from the pore size

Table 2. Results of the SAXS Analysis

sample	ratio silica/polymer	l_p[a] [nm]	S[a] [m^2/g]	$g(0)$[a]	R_{sphere}[b] [nm]	S_{theo}[b] [m^2/g]
mpPBI-1	0.303	6.41	67	0.115	6.7	56
mpPBI-2	0.424	6.66	71	0.108	6.7	63
mpPBI-3	0.545	7.08	108	0.064	6.7	114
mpPBI-4	0.667	7.29	116	0.055	6.7	131
mpPBI-5	0.788	7.03	126	0.055	6.7	140
mpPBI-6	1.030	6.99	163	0.048	6.7	203
mpPBI-7	1.273	5.84	130	0.075	5	151

[a] Determined by the parametrization approach. [b] Determined by applying the model for noninteracting hard spheres.

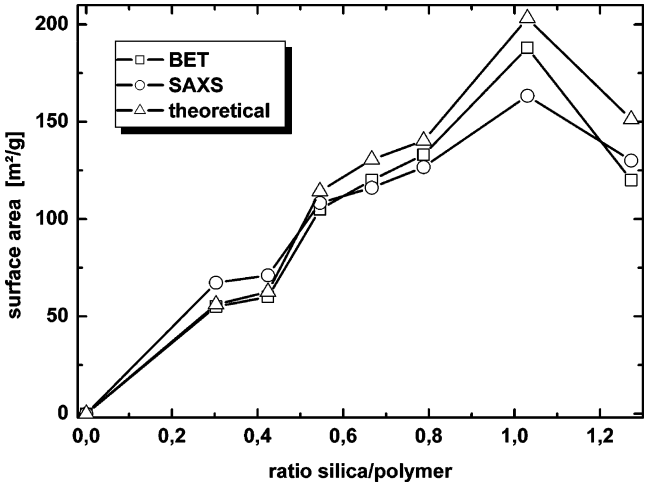

Figure 6. Specific surface area as a function of the template content.

determined by the form factor minimum and the total pore volume determined by N_2-sorption shows the absence of micropores (compare Figure 6).

The Porod length is not only connected to the inner surface of the sample but also to the average pore size. There are two relationships that connect the pore size with the Porod length:

$$R_{pore} = \frac{3}{4} l_p \tag{3}$$

$$\frac{1}{l_p} = \frac{1}{(1-\phi) l_{pore}} = \frac{1}{\phi l_{wall}} \tag{4}$$

Equation 3 accounts for the case that the scattering is due to "isolated" spheres, while (4) allows the calculation of the average pore size l_{pore} and the average wall thickness l_{wall} without assuming certain pore morphology. However, eq 4 fails at low porosities ($\phi < 0.3$), while eq 3 fails at high porosities ($\phi > 0.3-0.4$). Taking this into account, we determined the average pore size from l_p. We found, independent of the template content, values varying between 10 and 11 nm.

These are smaller values than those determined by TEM measurements. The fact that the pore sizes are smaller than those determined by TEM can be attributed to the presence of small

Table 3. Results of the Nitrogen Sorption and SAXS Measurements of Mesoporous PBI with Varying Content of Cross-linker

sample	mol % cross-linker[a]	S (BET) [m^2/g]	ϕ_{pore}	l_p [nm]	S (SAXS) [m^2/g]	l_{pore}[b] [nm]	$g(0)$
mpPBI-6	66.6	188	0.371	6.99	163	11.1	0.048
mpPBI-8	50	150	0.303	6.27	148	9.6	0.071
mpPBI-9	40	141	0.295	6.83	133	9.7	0.071
mpPBI-10	30	156	0.329	6.30	161	9.5	0.087
mpPBI-11	20	152	0.317	6.57	149	9.6	0.063
mpPBI-12	10	76	0.182	7.37	76	9.0	0.025
mpPBI-13	0	1	0.011	8.97	4		0.085

[a] With respect to 3,3′-diaminobenzidine. [b] Using eq 6.

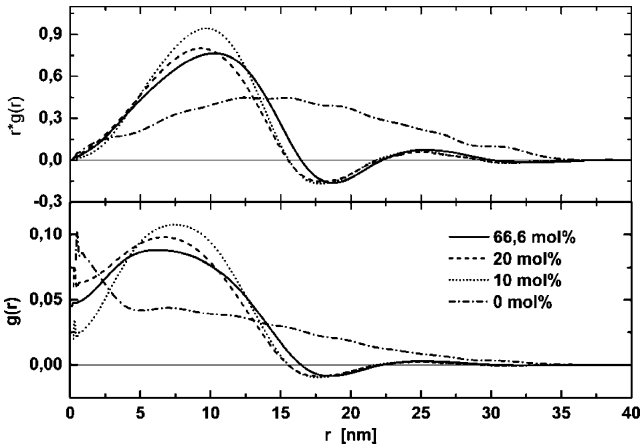

Figure 7. $g(r)$ and r•$g(r)$ plot of samples with varying cross-linking density.

pores, which are not visible by TEM but they account to the inner surface and thus to l_p. The BJH model gives too small values, which is due to the underlying model of cylindrical pores.[38,39] However, it can be concluded that the pore diameter in the polymer is systematically smaller than the diameter of the template (12.7 nm by SAXS). As the hard silica template stays unchanged during the synthesis this can be attributed to pore shrinking and the onset of pore collapse in this system.

Variation of the Cross-Linking Density. Since PBI is considered to be a rigid polymer, it might be possible that the inherent stiffness prevents the polymer from pore collapsing. Thus, the effect of the cross-linking density on the final structure of the pore system was investigated. This was achieved by co-polycondensation of different cross-linker/linear extender mixtures at a constant polymer/silica ratio of 1.03. Table 3 shows the applied compositions plus quantitative results of nitrogen sorption and SAXS measurements. Again a perfect agreement between the surface areas determined by the BET model and SAXS was found. As shown above, the average pore size is best described by SAXS. The highest porosity is achieved for a fully cross-linked network (corresponding to 66.6 mol % of the cross-linker with respect to 3,3′-diaminobenzidin), while practically no porosity is found for non-cross-linked samples. Furthermore, the pore size is independent of the content of cross-linker.

Both techniques reveal that the surface area and overall porosity increases with the amount of cross-linker until a final constant behavior is reached at a cross-linker content of about 20 mol %. This amount is sufficient to stabilize a hard and mechanically robust PBI framework ensuring a sustainable replication of the hard templates.

Figure 7 shows the chord length distribution $g(r)$ together with the r•$g(r)$ plot of the samples with varying cross-linker content. This presentation of the data reveals that the linear PBI exhibits not only weak but also ill-defined porosity: the channel system has essentially collapsed. At 10 mol % cross-linker content, we already observe well-defined pores of the same size as the template, however to a lower extent. The explanation for this behavior can only be given by considering a slightly inhomogeneous cross-linking density, making the pores either collapse or noncollapse. Pore collapse is, due to the involved capillary pressures, a critical phenomenon: the pores either vanish completely, or they stay open. The smaller $g(0)$ value for the lowly cross-linked samples is a measure for lower surface roughness or lower microporosity,[37] both of which are obviously related to the molecular steric demands and connection patterns of the cross-linker.

Conclusions

A solvent mediated hard-templating procedure using silica nanoparticles as template was developed for the synthesis of highly porous, cross-linked poly(benzimidazoles) with a well-defined mesoporous structure. The resulting materials were characterized by nitrogen sorption measurements, TEM, and quantitative SAXS measurements. The polymer exhibits a disordered pore structure, which reflects the homogeneous, gaslike distribution of the silica nanoparticles during the synthesis. We however believe that the disordered system is sufficient for the needs of membrane technology or catalysis, which do not directly profit from a mesoscopic order.[40]

The porosity and surface area of the PBIs can be tuned by varying the silica/polymer ratio, while the highest available porosity is observed for a silica/polymer ratio of 1. Further increase of the silica content leads to a lower porosity and less defined pores because the pore walls getting too thin to withstand the emerging high interfacial forces. It should be mentioned that even though the silica particles used in this contribution were of constant diameter, there is no visible restriction on the template size; i.e., various diameters of silica templates will surely enable mesoporous PBI's with varying pore sizes using this approach.

It was shown that 20 mol % cross-linker is at least needed for the complete replication of the template. Below this value, the PBI behaves as a ductile, linear polymer closing the pores by capillarity. Above this value and up to complete cross-linking, exact replication of the primary template structure is found. This observation also enables a potential functionalization of the PBI structures via copolymerization with functional co-monomers, which would be beneficial for the use of such systems in catalysis and proton membrane technology.

The presented mesoporous polybenzimidazoles might find applications as membrane materials in PEMFCs. Because of the increased porosity of the polymers, high acid uptakes can be expected. Also the pores can act as nanoreactors for, e.g., polymerizations, enabling new polymer−polymer nanocomposites of otherwise immiscible polymers.

Experimental Section

Synthesis of Benzene-1,3,5-tricarboxylic Acid Triphenyl Ester. To a solution of phenol (10.00 g, 0.106 mol) in a mixture

of 20 mL of pyridine and 50 mL of tetrahydrofuran (THF) was added dropwise at 0 °C a solution of 1,3,5-tribenzoyl chloride (9.4 g, 0.035 mol) in 20 mL of THF. The mixture was stirred at room temperature for 18 h under an argon atmosphere. The slurry was poured into 100 mL of iced water afterward. The mixture was acidified with concentrated hydrochloric acid and the product was separated by filtration. It was purified by washing with water, diluted hydrochloric acid, and water. The crude product was recrystallized from ethanol to yield a white solid.

^{1}H NMR ($CDCl_3$): $\delta = 9.25$ (s, 1H), 7.48 (t, 2H, $J = 7.88$ Hz), 7.48 (t, 2H, $J = 7.38$ Hz), 7.48 ppm (t, 2H, $J = 8.36$ Hz). ^{13}C NMR ($CDCl_3$): $\delta = 163.5, 150.7, 136.2, 129.8, 126.5, 121.7$ ppm. mp = 169−170 °C

LUDOX-Templated Poly(benzimidazole). Stoichiometrically exact mixtures of 3,3′-diaminobenzidine, diphenyl isophthalate, and/or benzene-1,3,5-tricarboxylic acid triphenyl ester were prepared in a round-bottom flask. The LUDOX HS-40 dispersion was added to the mixture, followed by the addition of 5−8 mL of DMF (depending on the amount of LUDOX) while stirring. The heterogeneous mixture was heated under argon flow with stirring to 150 °C. At around 80 °C the mixture becomes a clear, brown solution. At 150 °C the pressure was reduced to 300 mbar and subsequently to 200 mbar, while the temperature was allowed to increase to 170 °C. After all DMF has been removed from the flask, the pressure was reduced to 50 mbar and the temperature was increased to 200 °C. After 1.5 h at these conditions, the mixture was cooled to room temperature under an argon atmosphere. The resulting solid was heated to 400 °C under a protective gas atmosphere (N_2) for 30 min to complete the condensation. Removal of the silica particles was obtained by immersion of the composite in 50 mL of 4 M NH_4HF_2 solution for 3 days. Finally the polymers have been washed with water, ethanol, and acetone and dried *in vacuo*.

Measurements. The IR spectra were collected with a BIORAD FTS 6000 FTIR spectrometer, equipped with an attenuated total reflection (ATR) setup. Thermogravimetric analysis has been carried out using a NETZSCH TG209. The heating rate was 20 K/min. The measurements were carried out under an air atmosphere.

Transmission electron microscopy (TEM) images of microtomed samples were taken with a Zeiss EM 912Ω at an acceleration voltage of 120 kV.

SAXS curves were recorded at room temperature with a Nonius rotating anode instrument (4 kW, Cu Kα) with pinhole collimation and a MARCCD detector (pixel size: 79). The distance between sample and detector was 74 cm, covering a range of the scattering vector $s = 2/\lambda \sin\theta = 0.04 - 0.7$ nm^{-1} (2θ = scattering angle, $\lambda = 0.154$ nm). 2D diffraction patterns were transformed into a 1D radial average of the scattering intensity. The influence of 3D-fluctuations on the scattering curve were calculated and eliminated from the scattering curve.[41] All scattering curves have been subjected to this procedure, so that the obtained scattering curves show the features of a near-ideal two phase system, and Porod law is observed.

Acknowledgment. We thank Dr. Bernd Smarsly for help with the discussion of the SAXS results. Financial Support from the ENERCHEM project is greatly acknowledged.

Supporting Information Available: Figures showing photographs of the reaction mixture, TEM micrographs of bulk mpPBI-3, evaluation of SAXS data, and nitrogen sorption data and a table of SAXS results. This material is available free of charge via the Internet at http://pubs.acs.org.

References and Notes

(1) Hentze, H. P.; Antonietti, M. *Rev. Mol. Biotech.* **2002**, *90*, 27.
(2) Antonietti, M.; Goltner, C.; Hentze, H. P. *Langmuir* **1998**, *14*, 2670.
(3) Antonietti, M.; Caruso, R. A.; Goltner, C. G.; Weissenberger, M. C. *Macromolecules* **1999**, *32*, 1383.
(4) Ahn, J. H.; Jang, J. E.; Oh, C. G.; Ihm, S. K.; Cortez, J.; Sherrington, D. C. *Macromolecules* **2006**, *39*, 627.
(5) Shastri, V. P.; Martin, I.; Langer, R. *Proc. Natl. Acad. Sci. U.S.A.* **2000**, *97*, 1970.
(6) Nam, Y. S.; Yoon, J. J.; Park, T. G. *J. Biomed. Mater. Res.* **2000**, *53*, 1.
(7) Cooper, A. I. *J. Mater. Chem.* **2000**, *10*, 207.
(8) Song, S.-W.; Torkelson, J. M. *J. Membr. Sci.* **1995**, *98*, 209.
(9) Shang, M. X.; Matsuyama, H.; Maki, T.; Teramoto, M.; Lloyd, D. R. *J. Appl. Polym. Sci.* **2003**, *87*, 853.
(10) Kiefer, J.; Hilborn, J. G.; Hedrick, J. L. *Polymer* **1996**, *37*, 5715.
(11) Di Luccio, M.; Nobrega, R.; Borges, C. P. *Polymer* **2000**, *41*, 4309.
(12) Kosonen, H.; Valkama, S.; Nykanen, A.; Toivanen, M.; ten Brinke, G.; Ruokolainen, J.; Ikkala, O. *Adv. Mater.* **2006**, *18*, 201.
(13) Meng, Y.; Gu, D.; Zhang, F. Q.; Shi, Y. F.; Cheng, L.; Feng, D.; Wu, Z. X.; Chen, Z. X.; Wan, Y.; Stein, A.; Zhao, D. Y. *Chem. Mater.* **2006**, *18*, 4447.
(14) Johnson, S. A.; Ollivier, P. J.; Mallouk, T. E. *Science* **1999**, *283*, 963.
(15) Kim, J. Y.; Yoon, S. B.; Kooli, F.; Yu, J. S. *J. Mater. Chem.* **2001**, *11*, 2912.
(16) Lu, A. H.; Kiefer, A.; Schmidt, W.; Schuth, F. *Chem. Mater.* **2004**, *16*, 100.
(17) Lu, A. H.; Schmidt, W.; Spliethoff, B.; Schuth, F. *Adv. Mater.* **2003**, *15*, 1602.
(18) Ryoo, R.; Joo, S. H.; Kruk, M.; Jaroniec, M. *Adv. Mater.* **2001**, *13*, 677.
(19) Groenewolt, M.; Thomas, A.; Antonietti, M. *Macromolecules* **2004**, *37*, 4360.
(20) Neuse, E. W. *Adv. Polym. Sci.* **1982**, *47*, 1.
(21) Xiao, L. *Chem. Mater.* **2005**, *17*, 5328.
(22) Li, Q. F.; He, R. H.; Jensen, J. O.; Bjerrum, N. J. *Chem. Mater.* **2003**, *15*, 4896.
(23) Hickner, M. A.; Ghassemi, H.; Kim, Y. S.; Einsla, B. R.; McGrath, J. E. *Chem. Rev.* **2004**, *104*, 4587.
(24) Mecerreyes, D.; Grande, H.; Miguel, O.; Ochoteco, E.; Marcilla, R.; Cantero, I. *Chem. Mater.* **2004**, *16*, 604.
(25) Vogel, H.; Marvel, C. S. *J. Polym. Sci.* **1961**, *50*, 511.
(26) Choe, E. W. *J. Appl. Polym. Sci.* **1994**, *53*, 497.
(27) Iwakura, Y.; Imai, Y.; Uno, K. *J. Polym. Sci., Part A: Gen. Pap.* **1964**, *2*, 2605.
(28) Goettmann, F.; Fischer, A.; Antonietti, M.; Thomas, A. *Angew. Chem. Int. Ed.* **2006**, *45*, 4467.
(29) Bouchet, R.; Siebert, E. *Solid-State Ionics* **1999**, *118*, 287.
(30) Brooks, N. W.; Duckett, R. A.; Rose, J.; Ward, I. M.; Clements, J. *Polymer* **1993**, *34*, 4038.
(31) Sing, K. S. W.; Everett, D. H.; Haul, R. A. W.; Moscou, L.; Pierotti, R. A.; Rouquerol, J.; Siemieniewska, T. *Pure Appl. Chem.* **1985**, *57*, 603.
(32) Smarsly, B.; Groenewolt, M.; Antonietti, M. *Prog. Colloid Polym. Sci.* **2005**, *130*, 105.
(33) Siemann, U.; Ruland, W. *Colloid Polym. Sci.* **1982**, *260*, 999.
(34) Percus, J. K.; Yevick, G. J. *Phys. Rev.* **1958**, *110*, 1.
(35) Ashcroft, N. W.; Lekner, J. *Phys. Rev.* **1966**, *145*, 83.
(36) Glatter, O.; Kratky, O. *Small-angle X-ray Scattering*; Academic Press: London, 1982.
(37) Smarsly, B.; Antonietti, M.; Wolff, T. *J. Chem. Phys.* **2002**, *116*, 2618.
(38) Kruk, M.; Jaroniec, M. *Chem. Mater.* **2001**, *13*, 3169.
(39) Coasne, B.; Gubbins, K. E.; Pellenq, R. J. M. *Particle Particle Syst. Characteriz.* **2004**, *21*, 149.
(40) Rolison, D. R. *Science* **2003**, *299*, 1698.
(41) Perret, R.; Ruland, W. *Kolloid Z. Z. Polym.* **1971**, *247*, 835.

MA062598M